the bulk synthesis of metal carbides having possibly unique structures and properties. The Mo_nC_{4n} clusters reported here are clearly not of the same general structure of the met-car class. Pilgrim and Duncan (*22*) have recently reported $Mo_8C_{12}^+$ ionic clusters presumably of the met-car class. Molybdenum carbide generally has the stoichiometry MoC or Mo_2C. Both of these carbides have long been known to be superconductive alloys with critical temperatures $T_c = 12.2$ K for Mo_2C and $T_c = 6.5$ and 9.26 K for MoC. Conductivity measurements of the Mo_nC_{4n} films produced in this study are currently under way. Efforts have begun to first purify and to further investigate the physical properties of the clusters reported here.

REFERENCES AND NOTES

1. A. Gedanken, M. B. Robin, N. A. Kneubler, *J. Phys. Chem.* **86**, 4096 (1982).
2. J. G. Eden, *Photochemical Vapor Deposition*, (Wiley, New York, 1992).
3. A. V. Dem'yanenko and A. A. Puretzky, *Spectrochim. Acta Part A* **46**, 509 (1990).
4. ______, *Sov. J. Quantum Electron.* **20**, 1437 (1990).
5. B. C. Guo, K. P. Kerns, A. W. Castleman Jr., *Science* **255**, 1411 (1992).
6. B. C. Guo, S. Wei, J. Purnell, S. Buzza, A. W. Castleman Jr., *ibid.* **256**, 515 (1992).
7. B. V. Reddy, S. N. Khanna, P. Jena, *ibid.* **258**, 1640 (1992).
8. S. F. Cartier, Z. Y. Chen, G. J. Walder, C. R. Sleppy, A. W. Castleman Jr., *ibid.* **260**, 195 (1993).
9. An Extrel (Madison, WI) FTMS-2000 Fourier transform mass spectrometer equipped with a Spectra-Physics DCR-11 pulsed yttrium-aluminum-garnet–Nd (YAG-Nd) laser (355 nm, 8-ns pulse width). For the FTMS experiments, the YAG-Nd laser was focused to a spot ~300 μm in diameter (10^6 to 10^7 W/cm^2) to desorb and simultaneously ionize the sample on the stainless steel disk. Although the power density of the laser radiation used to desorb and ionize the sample was kept low, it is possible that this desorption-ionization event produced some dissociation of the analyzed material. The resulting ions were then trapped and detected in the FTMS ion cell. Both positive and negative ions were examined in the region $m/z = 20$ to 4000. For most experiments, the ions were produced in the laser desorption event at a background pressure of 8×10^{-8} torr and then trapped for 3 to 20 ms before detection.
10. Mass spectra were obtained in this case with a VG-Analytical ZAB-EQ double-focusing magnetic sector–quadrupole hybrid instrument. Thermal desorption was accomplished by the resistive heating of a coiled Pt or Re wire.
11. Glow discharge mass spectra (positive ions) were obtained with a VG-9000 magnetic sector instrument. The glow discharge was established in an ionization region maintained with 1 torr of argon. Solid samples (<1 mg) were pressed onto indium pins. The discharge was established at 1000 V and ~1 mA of direct current. The glow discharge atomizes and ionizes the sample, and the resulting positive ions are extracted from the source region and separated by a magnetic sector before detection. The efficiency of the atomization and ionization processes are dependent on the elements to be examined and the physical nature of the sample. Best results are obtained when similar samples are used to provide calibration factors for the elements to be determined.
12. To perform the CID experiments, we isolated a selected parent ion in the FTMS cell and then accelerated that ion up to a center-of-mass collision energy of 5 to 20 eV in the presence of a static pressure of argon at 4×10^{-6} torr. Collisions between the molecular ion and the background argon gas resulted in the fragmentation of the accelerated ions. Multiple collisions of the excited ion with argon may have occurred before dissociation, especially at the low collision energies.
13. C. D. Cooper, W. F. Frey, R. N. Compton, *J. Chem. Phys.* **69**, 2367 (1978).
14. We found that TCNQ accepted electrons from I^- [EA (I) = 3.06 eV [S. G. Lias *et al.*, *J. Phys. Chem. Ref. Data* **17** (suppl. 1) (1988)] but did not react with Cl^- [EA (Cl) = 3.6 eV]. From this, we deduce that EA (TCNQ) = 3.3 ± 0.3 eV.
15. J. M. L. Martin, T. R. Taylor, J. Yustin, T. R. Burkholder, L. Andrews, *J. Phys. Chem.*, in press.
16. L. Andrews, in *Proceedings of the Second International Conference on Laser Ablation*, J. C. Miller and D. B. Geohegan, Eds. (American Institute of Physics, New York, in press).
17. R. W. Grimes and J. D. Gale, *Chem. Commun.* **1992**, 1222 (1992).
18. M. Methfessel, M. van Schilfgaarde, M. Scheffler, *Phys. Rev. Lett.* **71**, 209 (1993).
19. I. Dance, *Chem. Commun.* **1992**, 1779 (1992).
20. H. Chen, M. Feyereisen, X. P. Long, G. Fitzgerald, *Phys. Rev. Lett.* **71**, 1732 (1993).
21. J. S. Pilgrim and M. A. Duncan, *J. Am. Chem. Soc.* **115**, 4395 (1993).
22. R.E.H. acknowledges support by an appointment to the Oak Ridge National Laboratory Postdoctoral Research Associates Program administered jointly by the Oak Ridge Institute for Science and Education and the Oak Ridge National Laboratory. We are indebted to B. Sales for providing the x-ray fluorescence and magnetic susceptibility measurements reported herein. Research sponsored by the Directors Research and Development Fund, the Office of Health and Environmental Research, and the Office of Basic Energy Sciences, Oak Ridge National Laboratory, U.S. Department of Energy (DOE), under contract DE-AC05-84OR21400 with Martin Marietta Energy Systems, Inc. A.V.D., A.A.P., and the research at the Institute of Spectroscopy were supported, in part, by DOE. The University of Tennessee, Knoxville, Mass Spectrometry Center is supported by The Science Alliance, a State of Tennessee Center of Excellence.

6 July 1993; accepted 9 November 1993

Do Hydrofluorocarbons Destroy Stratospheric Ozone?

A. R. Ravishankara,* Andrew A. Turnipseed,† Niels R. Jensen, Stephen Barone,* Michael Mills,† Carleton J. Howard, Susan Solomon

Hydrofluorocarbons, many of which contain a CF_3 group, are one of the major substitutes for the chlorofluorocarbons and halons that are being phased out because they contribute to stratospheric ozone depletion. It is critical to ensure that CF_3 groups do not cause significant ozone depletion. The rate coefficients for the key reactions that determine the efficiency of the CF_3 radical as a catalyst for ozone loss in the stratosphere have been measured and used in a model to calculate the possible depletion of ozone. From these results, it is concluded that the ozone depletion potentials related to the presence of the CF_3 group in hydrofluorocarbons are negligibly small.

The global phase-out of the ozone-damaging chlorofluorocarbons (CFCs) and halons (chlorofluorobromocarbons) has led to various proposed substitutes. Many of the substitute compounds are hydrochlorofluorocarbons (HCFCs) and hydrofluorocarbons (HFCs). The short lifetimes of the HCFCs make them much less damaging to the ozone layer than the CFCs. The HFCs contain no chlorine or bromine, only fluorine. In contrast to chlorine and bromine, fluorine has been known to be benign toward the ozone layer. The HFCs have therefore been assumed to have ozone depletion potentials (ODPs) of essentially zero (*1*). (ODP is an index of the ozone depletion ability of a compound relative to CFC-11.) Under the U.S. Clean Air Act Amendments, only compounds with an ODP less than 0.2 may be used as halocarbon substitutes. The major HFCs under consideration or production are CF_3CFH_2 (134a), CF_3CF_2H (125), CHF_3 (23), CF_3CH_3 (143a), and CF_2HCH_3 (152a). In particular, HCFC-134a has begun to be widely used as a substitute for CFCs in air conditioning and refrigeration applications. Many of these HFCs contain a CF_3 functional group.

It has been recently suggested that molecules containing the CF_3 group may represent a special case of fluorine-catalyzed ozone loss (*2*). The CF_3 group is unusually stable and may destroy significant amounts of ozone through catalytic cycles involving CF_3O_x (CF_3O and CF_3OO) radicals (*2*). If this were true, many HFCs (and possibly a few currently acceptable HCFCs) could have ODPs greater than 0.2, and new substitutes would have to be developed. The consequences of such a radical change in scientific understanding for industry, international agreements, and the phase-out

---

National Oceanic and Atmospheric Administration, Aeronomy Laboratory, 325 Broadway, Boulder, CO 80303.

*Also affiliated with the Department of Chemistry and Biochemistry, University of Colorado, Boulder, CO 80309.

†CIRES, University of Colorado, Boulder, CO 80309.

of CFCs and HCFCs are far-reaching.

The important reactions of CF_3O and CF_3OO that may take place in the stratosphere are listed in Table 1. Reactions 1 and 2 constitute a catalytic cycle that is equivalent to $2O_3 \rightarrow 3O_2$. There are many other possible catalytic cycles that are represented by the list of reactions, some of which are equivalent to $2O_3 \rightarrow 3O_2$ and some to $O + O_3 \rightarrow 2O_2$.

All of the above catalytic cycles require that the CF_3 group stay intact. If the CF_3 group is degraded (as in reaction 3, for example), then the chain is terminated. In addition, reactions 4, 5, 8, and 11 lead to formation of CF_3 reservoirs, which can also produce some ozone depletion (for example, through the cycle represented by reactions 1, 11, and 12 in conjunction with reaction of OH with O_3). We have measured the rate coefficients for reactions 1 through 4, which are the key processes in these cycles, and used them to evaluate the ODPs of some of the most important HFCs that contain the CF_3 group.

A pulsed photolysis apparatus equipped with pulsed laser–induced fluorescence detection (3) as well as a low-pressure flow tube coupled to a chemical ionization mass spectrometer (CIMS) detector (4) were used to study reactions 1 through 4. Use of diverse methods helps to identify possible systematic errors and is essential in resolving an issue as critical as the present one.

In the pulsed photolysis apparatus, CF_3O radicals were generated by 193-nm laser photolysis of either bis-trifluoromethyl peroxide (CF_3OOCF_3) or $CF_3Br/O_2/NO$ mixtures. CF_3O was detected with laser-induced fluorescence by excitation of the $\tilde{A}(^2A_1) \leftarrow \tilde{X}(^2E)$ electronic transition at 350.2 nm (0-0 band). The detection limit for CF_3O (S/N = 1) was $<7 \times 10^9$ molecules cm^{-3} in 100 torr He upon averaging 100 laser shots. Typically, 10^{11} to 10^{12} molecules cm^{-3} of CF_3O were used. The delay time, that is, the reaction time, between the photolysis and the probe beam was varied between 10 μs and 50 ms to allow construction of the temporal profile of CF_3O.

In the flow tube apparatus, CF_3OO radicals were produced in a side-arm reactor by pyrolysis of CF_3I (producing CF_3, which reacts with O_2) and CF_3O by pyrolysis of CF_3OOCF_3. CF_3OO was reacted with I^- to produce CF_3O^- or with SF_6^- to generate CF_3OO^-. CF_3O was converted to CF_3O^- through its reaction with NO_3^- or SF_6^-. The ions were detected by a mass spectrometer. The reaction times were varied by moving an injector through which the stable reactants entered the flow tube. The detection limits for CF_3O and CF_3OO were $\sim 10^9$ molecules cm^{-3}. Typically, $\sim 5 \times 10^{10}$ molecules cm^{-3} of CF_3O and CF_3OO were used.

All experiments were carried out in a large excess of pure He under pseudo–first order conditions in the concentration of free radical that was monitored. The concentrations of the excess reagent such as O_3, NO, and CH_4 were determined as described elsewhere (4, 5). CF_3OOCF_3 and O_3 were measured by absorption at 184.9 nm and 254 nm (Hg lines), respectively.

For reaction 1, the temporal profiles of CF_3O in the presence of a large excess of O_3 were observed to be exponential. From these profiles, the first order rate coefficient $k_1' = (k_1[O_3] + k_d)$ was calculated. Here k_d is the first order rate coefficient for the loss of CF_3O in the absence of O_3. Within the errors, k_1' varied linearly with $[O_3]$ (Fig. 1). From these data, $k_1 = (2.5 \pm 1.0) \times 10^{-14}$ cm^3 $molecule^{-1}$ s^{-1} at 298 K was determined in the pulsed photolysis system. The flow-tube study yields a consistent value ($k_1 < 4 \times 10^{-14}$ cm^3 $molecule^{-1}$ s^{-1}). To be conservative in the ODP calculations, we

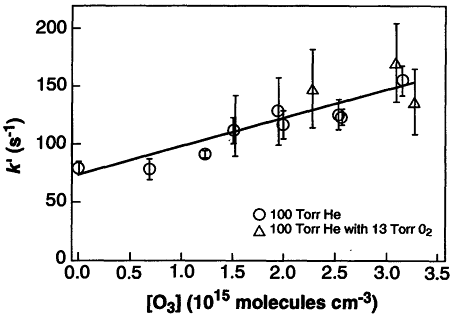

Fig. 1. A plot of the measured first order rate coefficient for the loss of CF_3O radicals measured with the pulsed photolysis system in the presence of various amounts of O_3. The slope of the line is k_1 and the intercept is the first order rate coefficient for loss of CF_3O in the absence of O_3. The open triangles were measured in the presence of 13 torr of O_2.

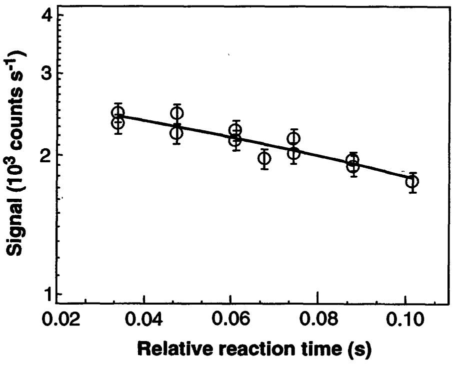

Fig. 2. A plot of CIMS signal produced by CF_3OO in the presence of 3.9×10^{15} molecules cm^{-3} of O_3 and a large amount of $(CH_3)_3CH$ to scavenge CF_3O as a function of relative reaction time. The slope of the line is the first order rate coefficient for the removal of CF_3OO; k_2 was calculated from slopes of such plots at various O_3 concentrations.

Table 1. The reactions and their rate coefficients important in chemistry of CF_3 in the stratosphere and used for modeling the effect of CF_3 on the ODP of HFCs. For the model calculations, the rate coefficients and reaction products are selected so as to maximize the estimated ozone depletion.

Reaction	Rate constant (cm^3 $molecule^{-1}$ s^{-1})	Comments
1. $CF_3O + O_3 \rightarrow CF_3O_2 + O_2$	$<4 \times 10^{-14}$	This work, upper limit
2. $CF_3O_2 + O_3 \rightarrow CF_3O + 2O_2$	$<3 \times 10^{-15}$	This work, upper limit
3. $CF_3O + NO \rightarrow CF_2O + FNO$	6×10^{-11}*	This work, 298 K. Higher at lower *T*
4. $CF_3O + CH_4 \rightarrow CF_3OH + CH_3$	$>2 \times 10^{-15}$	This work, extrapolated to low *T*
5. $CF_3O_2 + NO_2 + M \rightarrow CF_3O_2NO_2 + M$		(*6*)
6. $CF_3O_2NO_2 + h\nu \rightarrow CF_3O + NO_3$		Assumed to be same as HO_2NO_2 cross sections (*6*)
7. $CF_3O_2 + O \rightarrow CF_3O + O_2$	6×10^{-11}	Estimated; similar to $HO_2 + O$
8. $CF_3O + ClO + M \rightarrow CF_3OOCl + M$	2×10^{-11}	High-pressure bimolecular limit
9. $CF_3OOCl + h\nu \rightarrow CF_3O_2 + Cl$		Use Cl_2O_2 cross sections (*6*)
10. $CF_3O_2 + ClO \rightarrow CF_3O + Cl + O_2$	5×10^{-12}	Same as CH_3O_2 + ClO in (*6*)
11. $CF_3O_2 + HO_2 \rightarrow CF_3OOH + O_2$	3.8×10^{-13} exp(800/*T*)	Assumed to be same as $CH_3O_2 + HO_2$
12. $CF_3OOH + h\nu \rightarrow CF_3O + OH$		Assumed to be same as CH_3OOH (*6*)
13. $CF_3OO + NO \rightarrow CF_3O + NO_2$	1.5×10^{-11}	(*4*) and this work

*Very recent results from our laboratory show that this rate coefficient increases slightly at lower temperatures. The previously reported value, $k_3 = (2 \pm 1) \times 10^{-11}$ cm^3 $molecule^{-1}$ s^{-1} from our laboratory (*4*), was estimated by modeling the CF_3O profiles in the CF_3OO + NO reaction system and is superseded by the present direct determination.

used an upper limit of 4 × 10^{-14} cm^3 $molecule^{-1}$ s^{-1} for this rate coefficient (Table 1). Our other observations are consistent with the products of this reaction being CF_3OO and O_2 (see below). This reaction will likely be slower in the stratosphere, where the temperature will be much lower.

For reaction 2, the temporal profile of CF_3OO was measured in the flow tube equipped with chemical ionization mass spectrometry (CIMS) detection in excess O_3 (Fig. 2). As a means to inhibit the possible regeneration of CF_3OO by the reaction of the product CF_3O with O_3, isobutane was added in great excess to scavenge the CF_3O product through the reaction $CF_3O + (CH_3)_3CH \rightarrow CF_3OH + (CH_3)_3C$. The loss of CF_3OO was very small in an excess of O_3 (1.5 × 10^{15} to 5.0 × 10^{15} cm^{-3}) when the isobutane scavenger was present; this indicates a very slow reaction, $k_2 < 3 \times 10^{-15}$ cm^3 $molecule^{-1}$ s^{-1}, if indeed any reaction does occur at all. In the absence of the CF_3O scavenger, the temporal profile of CF_3OO showed no loss, which suggests that if the slow reaction were occurring, it produces CF_3O that in turn reacts with O_3 to regenerate CF_3OO. A low value of k_2 is consistent with the low reactivity with O_3 of other peroxy radicals such as HO_2 ($k = 2 \times 10^{-15}$ cm^3 $molecule^{-1}$ s^{-1}) and CH_3OO ($k < 3 \times 10^{-17}$ cm^3 $molecule^{-1}$ s^{-1}) (6). An upper limit for k_2 at 298 K was also deduced from pulsed photolysis, where the ratio of k_1/k_2 was measured to be >4. On the basis of the quoted upper limit for k_1, we calculate $k_2 < 1 \times 10^{-14}$ cm^3 $molecule^{-1}$ s^{-1}, consistent with the CIMS value. This rate coefficient is likely to be lower at stratospheric temperatures on the basis of analogy with the HO_2 reaction.

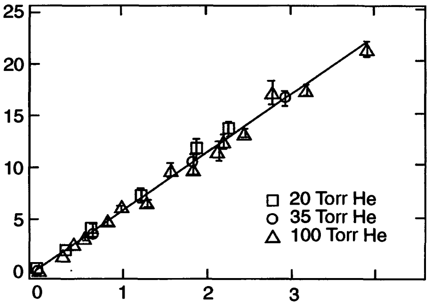

Fig. 3. A plot of the measured first order rate coefficient for the loss of CF_3O radicals as measured with pulsed photolysis system in the presence of various concentrations of NO. The slope of the line is k_3 and the intercept is the first order rate coefficient for loss of CF_3O in the absence of NO. Data represented by various symbols were obtained under pressure conditions as shown in the legend.

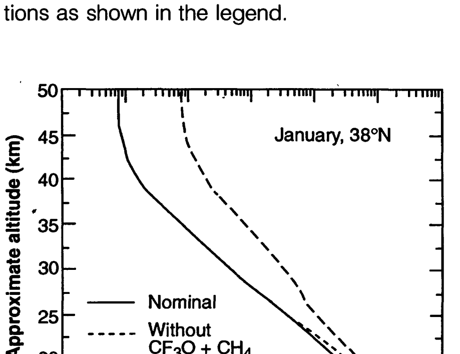

Fig. 4. Calculated efficiency of CF_3 radicals released from HFCs for ozone loss relative to chlorine released from CFCs, as a function of altitude, for mid-latitudes in winter. Three model cases are shown: (i) a nominal case in which the chemical scheme of Table 1 is used (except for the reaction between CF_3O and ClO, see text); (ii) a case where the reaction between CF_3O and CH_4 is neglected for the purpose of illustration; and (iii) a case where the rate constant for the reaction between CF_3O and NO is reduced by a factor of 10.

For reaction 3, the temporal profiles of CF_3O measured in the photolysis system were strictly exponential and gave the values of the first order rate coefficient $k_3' = (k_3[NO] + k_d)$. In this expression, k_d is the first order loss rate coefficient of CF_3O in the absence of NO. A plot of k_3' versus [NO] from one series of experiments is shown in Fig. 3. The slope of this line is k_3 and yields a value of $k_3 = (5.45 \pm 0.57) \times 10^{-11}$ cm^3 $molecule^{-1}$ s^{-1}. Similar experiments carried out in the flow tube yield $k_3 = (5.7 \pm 1.3) \times 10^{-11}$ cm^3 $molecule^{-1}$ s^{-1}. In the pulsed photolysis system, k_3 and k_{13} were also measured by production of CF_3O from CF_3Br photolysis in the presence of NO and O_2 to be (5.46 ± 0.68) × 10^{-11} and (1.57 ± 0.38) × 10^{-11} cm^3 $molecule^{-1}$ s^{-1}, respectively. This value of k_{13} is in good agreement with previous determinations (4). The agreement between these three determinations of k_3 is excellent and yields an average value of $k_3 = (5.6 \pm 0.7) \times 10^{-11}$ cm^3 $molecule^{-1}$ s^{-1}, independent of pressure. The products of this reaction have been shown to be CF_2O + FNO (4, 7, 8). Preliminary measurements show that the rate coefficient for this radical-radical reaction increases slightly with decreases in temperature. Thus, the rate coefficients at stratospheric temperatures will be larger than the 298 K value (Table 1).

For reaction 4, k_4 was also measured by following CF_3O loss in the pulsed photolysis system as well as in the CIMS system in the presence of a large excess of CH_4. The averaged 298 K value was (2.1 ± 0.4) × 10^{-14} cm^3 $molecule^{-1}$ s^{-1}, in good agreement with another recent measurement (9). Extrapolation of a few measured values of k_4 at temperatures above 245 K to lower stratospheric temperatures of 200 K yields the lower limit shown in Table 1.

Estimates of the other rate coefficients needed to assess the role of CF_3 in the stratosphere are given in Table 1. In the modeling calculations described below, it is assumed that CF_3 is released instantaneously upon initiation of HFC degradation, primarily by OH or $O(^1D)$ reactions, and converted into CF_3OO in the atmosphere. All of the rate coefficients and photochemical parameters shown in Table 1 are either measured or estimated on the basis of analogies.

We evaluated the ODPs of several HFCs containing the CF_3 group using both semiempirical and purely theoretical approaches (*10, 11*). The purely theoretical calculations were carried out with a two-dimensional (latitude and altitude) numerical model of the atmosphere (*10*) wherein perturbations of the HFC in question and a reference gas (CFC-11) are considered and the relative ozone loss is determined. The model includes heterogeneous chemistry on sulfate aerosols but not polar stratospheric clouds. All of the CF_3-related species (see Table 1) were calculated from steady-state assumptions, and the chemistry of Table 1 was adopted with two important exceptions: (i) Reaction 8 (CF_3O + ClO) was not considered because the present model does not include polar stratospheric cloud chemistry and related polar ozone depletion processes and (ii) the production of ozone by photolysis of NO_2 formed from reaction 13 was neglected to maximize the possible ozone loss and, hence, present a worst case. Sensitivity tests were also carried out to ensure that reaction 8 is not significant as compared with others that were included and, therefore, not a serious shortcoming. For the semiempirical calculations, the distribution of the HFC source gas 134a was inferred from an observationally derived CH_4 distribution in which the correlation of HFC-134a with CH_4 determined from the two-dimensional model was used. The relative efficiency of CF_3 released from HFC-134a for ozone loss as compared with chlorine released from CFCs was evaluated in the two-dimensional model and used as input to the semiempirical calculation. Figure 4 shows the value of this important parameter (hereafter referred to as ε), illustrating the fact that the CF_3 radicals are most efficient for ozone loss relative to chlorine in the lowest part of the stratosphere. This result might be expected from the fact that CF_3O and CF_3OO are chemically similar to OH and HO_2.

Table 2 presents the ODPs calculated for HFC-134a, -23, and -125. The lifetimes of these three species are between about 15 and 400 years, bracketing the range for the important HFCs. For the semiempirical calculations, a range of possible ozone loss profiles based on measurements was adopted as described in Solomon *et al.* (*11*). The table shows the highest values derived as an upper limit, which were obtained when no vortex processing was considered and maximum ozone changes were adopted at the lowest altitudes; see Solomon *et al.* (*11*). The semiempirical values are similar to those of the complete model but tend to be somewhat larger, owing mainly to the fact that the theoretical model tends to underestimate the observed ozone losses in the lowest part of the stratosphere. The semiempirical calculation includes only observed ozone losses above ~12 km; as Table 2 indicates, losses at lower altitudes do play a role in the theoretical model calculations. The calculated ODPs for HFC-125 and HFC-23 are greater than that of HFC-134a because of their longer lifetimes, but are still found to be well below 1×10^{-3}.

We next present a calculation showing the expected benefit to the ozone layer of substitution of HFC-134a for current CFC use. The calculation is intended to be illustrative rather than realistic. A comparison of the calculated ozone loss rates resulting from different chemical processes for mid-latitudes (Fig. 5) shows that the shape of the ozone loss profile related to CF_3 chemistry is similar to that of $OH + O_3$ and $HO_2 + O_3$ and is much steeper than that of chlorine-related chemistry (compare with Fig. 4). Figure 5 shows that the ozone depletion related to the reservoirs considered (CF_3OOH and CF_3OONO_2) is negligible. Indeed, if these reservoirs are short-lived (that is, an instantaneous balance between production and loss can be assumed in the stratosphere) and their ozone destruction can be neglected, then they play no role in determining the ODP. To obtain a globally averaged ozone loss of ~1% that is illustrated in Fig. 5, an HFC-134a tropospheric abundance of 1 ppmv was needed. Such a large, albeit unrealistic, abundance was used to ensure the accuracy of the calculated O_3 change and, more importantly, to show that a very large total global release of HFC-134a of about 1.5 billion metric tons per year would be required to produce a globally averaged ozone loss of ~1%. This number can be compared to the global use of all CFCs, estimated at about 700,000 metric tons in 1991. This calculation therefore implies that even in the case of complete substitution of HFC-134a for all CFC use, ozone depletion would be expected to be markedly reduced.

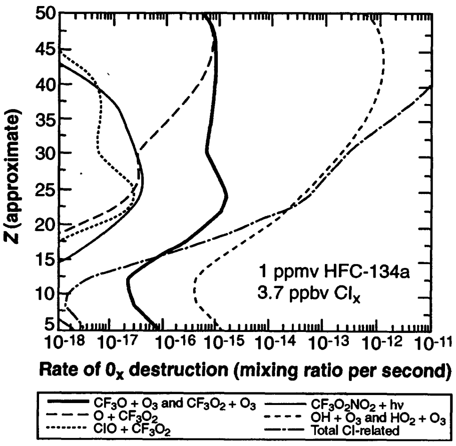

Fig. 5. Calculated ozone loss rates (mixing ratio per second) versus altitude for mid-latitude winter for different chemical processes. Note that these calculations assume a very large tropospheric abundance of 1 ppmv of HFC-134a.

In addition to the O_3 loss mechanisms and CF_3O_x reactions that we have explicitly considered, there are other proposed cycles and reactions that may affect the chemistry of CF_3O_x in the stratosphere. The cycle involving the reaction of O with CF_3O, proposed by Li and Francisco (*12*), is one such scheme. Our measured value of k_3 is close to that possible for the reaction of CF_3O with O, and the abundance of NO will exceed that of O atoms below ~40 km. Further, if the products of the $CF_3O + O$ reaction are $CF_2O + FO$, this reaction will terminate, rather than propagate, the catalytic chain. Therefore, this reaction scheme was not included here. Similarly, we have neglected the reaction of CF_3O with O_2, which will lower the calculated efficiency of CF_3 in destroying O_3 because it will generate CF_2O. The chemistry of FNO has not been included, because it absorbs quite strongly in the 290 to 340 nm region (*13*) and, hence, will photolyze rapidly to F and NO. The F atoms will be quickly converted to HF through reactions with CH_4, H_2O, and so forth in the stratosphere.

Table 2. Calculated ozone depletion potentials (ODPs) for various hydrofluorocarbons.

Molecule	Lifetime (years)	Notes*	ODP	
			Full model	Semiempirical
HFC-134a	15.4	As in Table 1; all altitudes	1.5×10^{-5}	
		As in Table 1; $z \geq 10$ km	1.3×10^{-5}	2.4×10^{-5}
		As in Table 1; $z \geq 16$ km	7.8×10^{-6}	
		$(CF_3O + NO)/10$; $z \geq 10$ km	3.0×10^{-5}	7.5×10^{-5}
		$CF_3O + CH_4 = 0$; $z \geq 10$ km	4.0×10^{-5}	
		$(CF_3O + NO)/10$; CF3O + $CH_4 = 0$; $z \geq 10$ km; large polar ozone losses		4.8×10^{-4}
HFC-23	405	As in Table 1, all altitudes	3.9×10^{-4}	
		As in Table 1, $z \geq 10$ km	3.5×10^{-4}	
		As in Table 1, $z \geq 16$ km	1.5×10^{-4}	
HFC-125	40.5	As in Table 1, all altitudes	3.0×10^{-5}	
		As in Table 1, $z \geq 10$ km	2.6×10^{-5}	
		As in Table 1, $z \geq 16$ km	1.5×10^{-5}	

*z is the altitude (in kilometers).

The calculations presented here show that the ozone depletion caused by the HFCs should be greatest in the lower stratosphere. The ODP depends primarily on the rate constant for the reaction of CF_3O with O_3 (which causes ozone loss) as compared to the reactions of CF_3O with NO and CH_4 (which terminate the catalytic cycle; Fig. 4 illustrates that both are important in the lower stratosphere). Thus, the results presented here depend to some extent on the modeled NO distribution. An extreme sensitivity test was therefore carried out in which the rate constant for the reaction of CF_3O with NO (or, alternatively, the NO concentration) was decreased by a factor of 10. As can be seen from Table 2, even in this case the calculated ODP of HFC-134a for both the semiempirical and theoretical models is less than 1×10^{-4}. Similarly, in the extreme case of neglecting completely the reaction of CF_3O with CH_4 (or, equivalently, assuming that the product CF_3OH is short-lived and regenerates CF_3), an ODP of about 4×10^{-5} is estimated for HFC-134a from the theoretical model. The most extreme case considered was one in which the reaction of CF_3O with CH_4 was neglected, the reaction of CF_3O with NO was divided by a factor of 10, and large polar ozone losses were included in the semiempirical model. Even for this very unrealistic simulation, the estimated ODP for HFC-134a was less than 5×10^{-4}, largely because the rate of formation of CF_3 is slow in the high-latitude lower stratosphere and because chlorine chemistry is quite effective at destroying ozone there.

The kinetics measurements described here together with modeling and semiempirical estimates show that the chemical reactions involving CF_3O and CF_3OO lead to negligibly small ODPs. Therefore, we conclude that HFCs and HCFCs containing CF_3 groups are no more harmful to the stratospheric ozone layer than those that do not. For example, the ODP for HCFC-123 will be determined by its chlorine release, with the presence of the CF_3

group making essentially no contribution to the total. On the basis of our current understanding, it appears highly likely that the ODPs for the HFCs considered here are all well below 1×10^{-3}. For the key substitute HFC-134a, the best estimate of the ODP is only 1×10^{-5} to 2×10^{-5}.

Note added in proof: Since the submission of this manuscript, several studies on reaction 1 (*14–16*), reaction 2 (*14, 15*), reaction 3 (*17*), and reaction 13 (*17*) have been published. All of these measurements are in agreement with the results reported here.

REFERENCES AND NOTES

1. World Meterological Organization (WMO), Scientific Assessment of Stratospheric Ozone: 1991 (1992).
2. P. Biggs *et al.*, paper presented at STEP-HALOCIDE/AFEAS Workshop, University College, Dublin, Ireland, 23 to 25 March 1993.
3. A. A. Turnipseed, S. B. Barone, A. R. Ravishankara, *J. Phys. Chem.* **96**, 7502 (1992).
4. T. B. Bevilacqua, D. R. Hanson, C. J. Howard, *ibid.* **97**, 3705 (1993).
5. A. A. Turnipseed, S. B. Barone, A. R. Ravishankara, *ibid.*, p. 5926.
6. W. B. DeMore *et al.*, Jet Propulsion Laboratory, Chemical Kinetics and Photochemical Data for Use in Stratospheric Modeling (1992).
7. Z. Li and J. S. Francisco, *Chem. Phys. Lett.* **186**, 336 (1991).
8. J. Chen, T. Zhu, H. Niki, *J. Phys. Chem.* **96**, 6615 (1992).
9. H. Saathoff and R. Zellner, *Chem. Phys. Lett.* **206**, 349 (1993).
10. R. R. Garcia, F. Stordal, S. Solomon, J. T. Kiehl, *J. Geophys. Res.* **97**, 12967 (1992).
11. S. Solomon *et al.*, *ibid.*, p. 825.
12. Z. Li and J. S. Francisco, *Chem. Phys. Lett.* **209**, 151 (1993). The ozone destruction cycle proposed by these authors [$CF_3O + O \rightarrow CF_3 + O_2$, $CF_3 + O_2 \rightarrow CF_3OO$, $CF_3OO + NO \rightarrow CF_3O + NO_2$, $NO_2 + O \rightarrow NO + O_2$] is not effective, because NO_2 predominately photolyzes to NO + O, creating a null cycle.
13. H. S. Johnston and H. J. Bertin, *J. Mol. Spectrosc.* **3**, 683 (1959).
14. O. J. Nielsen and S. Sehested, *Chem. Phys. Lett.* **213**, 433 (1993).
15. M. Maricq and J. J. Szente, *ibid.*, p. 449.
16. T. J. Wallington, M. D. Hurley, W. F. Schneider, *ibid.*, p. 442.
17. J. Sehested and O. J. Nielsen, *ibid.* **206**, 369 (1993).
18. Funded in part by NOAA Climate and Global Change program and by the Alternative Fluorocarbons Environmental Acceptability Study (AFEAS). We are grateful to D. Dixon, the du Pont de Nemours Co., AFEAS, and D. DesMarteau for providing CF_3OOCF_3. We appreciate helpful discussions with D. Hanson at CIRES and N. D. Sze of AER, Inc. N.R.J. is a Postdoctoral Research Associate of the Danish National Science Research Council.

3 September 1993; accepted 4 November 1993

Target of the Transcriptional Activation Function of Phage λ cI Protein

Mei Li, Henry Moyle, Miriam M. Susskind*

Activation of transcription initiation by the cI protein of phage λ is thought to be mediated by a direct interaction between cI and RNA polymerase at the P_{RM} promoter. Two negatively charged amino acid residues in the DNA binding domain of cI play a key role in activation, suggesting that these residues contact RNA polymerase. The subunit of RNA polymerase involved was identified by selecting polymerase mutants that restored the activation function of a mutant form of cI protein. Although previous studies suggest that several activators interact with the α subunit of RNA polymerase, the results here suggest that cI interacts with the σ subunit. An arginine to histidine change near the carboxyl terminus of σ specifically suppresses an aspartic acid to asparagine change in the activation region of cI. This finding supports the direct-contact model and suggests that a cluster of positively charged residues near the carboxyl terminus of σ is the target of the negatively charged activation region of cI.

Gene expression is frequently regulated by activator proteins that stimulate the rate of transcription initiation at specific promoters. In many cases, activation is thought to involve direct contact between the activator and RNA polymerase on the promoter DNA. Strong evidence for this model has been presented for the *cI* gene product of phage λ, which acts as both a repressor and activator of transcription (*1*). In λ lysogens, cI protein binds to sites in the O_R and O_L operators, thereby turning off two major promoters, P_R and P_L. At the same time, the cI dimer bound to O_R2 turns on transcription of the *cI* gene from the P_{RM} promoter (Fig. 1). The cI dimer bound to O_R2 is thought to interact directly with RNA polymerase bound to P_{RM}, thereby stimulating isomerization of closed polymerase-promoter complexes to open complexes (*2–6*). Part of the evidence for this model was the isolation of a special class of *cI* mutants, called *pc* for positive control, that bind to O_R and repress P_R normally, but cannot activate P_{RM} (*3–6*). The *pc* mutations change amino acids in the first α helix or turn of the helix-turn-helix DNA binding motif of cI. These residues are on the surface of the cI DNA binding domain when it is bound to operator DNA (*7*) and are appropriately positioned to contact RNA polymerase (*4*).

The region of RNA polymerase that contacts cI protein was unknown. The major form of *Escherichia coli* RNA polymerase is composed of a core enzyme $(\alpha_2\beta\beta')$ plus the dissociable σ^{70} subunit, which confers promoter specificity. The σ^{70} subunit is predicted to be close to cI, because σ^{70} recognizes the −35 region of the promoter (*8, 9*), which overlaps O_R2. The α subunit is another likely candidate to interact with cI, because α apparently interacts with several other activators (*10*). To identify which subunit is the target for activation by λ cI protein, we generated a mutant form of RNA polymerase that allows a cI-pc mutant to activate P_{RM}. To obtain this polymerase mutant, we constructed a strain carrying two P22 prophages integrated in the bacterial chromosome (Fig. 2). The first prophage (*11*) carries the *kan* (kanamycin resistance) gene under control of wild-type λ P_{RM}. The second

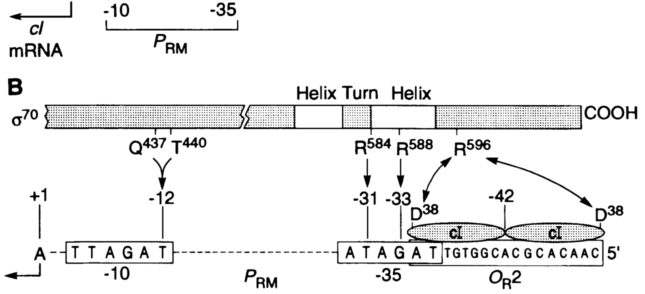

Fig. 1. (**A**) Organization of cI binding sites (open boxes) and promoter elements (filled boxes) in λ O_R region. In λ lysogens cI binds O_R1 and O_R2 (but not O_R3), represses P_R, and activates P_{RM}. (**B**) Proposed interactions between σ^{70} and the promoter or activator. The subunit σ^{70} is aligned with the leftward P_{RM} promoter with a cI dimer bound to O_R2. Arrows represent interactions between σ^{70} residues and consensus base pairs (*8, 9, 22*) (however, −31 of P_{RM} is nonconsensus) or the activation patch of cI. The latter interaction is presumably with the cI monomer at left. D, Asp; Q, Gln; R, Arg; T, Thr.

Department of Biological Sciences, University of Southern California, Los Angeles, CA 90089–1340.

*To whom correspondence should be addressed.